Structural characterization of *a*-plane $Zn_{1-x}Cd_xO$ ($0 \leqslant x \leqslant 0.085$) thin films grown by metal-organic vapor phase epitaxy

J. Zúñiga-Pérez[a] and V. Muñoz-Sanjosé
Departamento de Física Aplicada y Electromagnetismo, Universitat de València, C/ Dr. Moliner 50, 46100 Burjassot, Spain

M. Lorenz, G. Benndorf, S. Heitsch, D. Spemann, and M. Grundmann
Universität Leipzig, Fakultät für Physik und Geowissenschaften, Institut für Experimentelle Physik 11, Linnéstrasse 5, D-04103 Leipzig, Germany

(Received 27 July 2005; accepted 6 December 2005; published online 23 January 2006)

$Zn_{1-x}Cd_xO(11\bar{2}0)$ films have been grown on $(01\bar{1}2)$ sapphire (*r*–plane) substrates by metal-organic vapor phase epitaxy. A 800-nm-thick ZnO buffer, deposited prior to the alloy growth, helps to prevent the formation of pure CdO. A maximum uniform Cd incorporation of 8.5 at. % has been determined by Rutherford backscattering spectrometry. Higher Cd contents lead to the coexistence of $Zn_{1-x}Cd_xO$ alloys of different compositions within the same film. The near band-edge photoluminescence emission shifts gradually to lower energies as Cd is incorporated and reaches 2.93 eV for the highest Cd concentration (8.5 at. %). The lattice deformation, due to Cd incorporation, has been described using a new reference frame in which the lattice distortions are directly related to the *a*-plane surface structure. Cd introduction does not affect the *c* lattice parameter but expands the lattice along the two perpendicular directions, $[11\bar{2}0]$ and $[\bar{1}100]$, resulting in a quadratic volume increase. © *2006 American Institute of Physics*.
[DOI: 10.1063/1.2163014]

I. INTRODUCTION

Due to its high exciton binding energy (60 meV) and its wide band gap (3.37 eV), ZnO is currently considered as one of the most promising materials for use in optoelectronic devices operating at blue and ultraviolet wavelengths. Since the first reports on ZnO-based heterostructures the issue of band gap engineering, as a means to control the actual device emission energy, was addressed.[1–4] This wavelength tunability was accomplished by growing $Zn_{1-x}Mg_xO$ (Refs. 4–6) and $Zn_{1-x}Cd_xO$ (Refs. 4, 7, and 8) alloys, which show higher and lower band gap energies than ZnO, respectively. Besides, the fact that the lattice parameters of both alloys increase with higher Mg and Cd content allows a perfect in-plane lattice match for certain Mg and Cd concentrations, contrarily to what is found in the InGaN/AlGaN system.[4] However, owing to the different crystalline structure of the extreme binary compounds, with MgO and CdO exhibiting a rocksalt structure and ZnO a wurtzite one, phase separation was detected within the films.

Most of the studies dealt with *c*-plane oriented thin films. However, devices based on [0001]-oriented wurtzite materials are known to present spontaneous and piezoelectric electrostatic fields which spatially separate electrons and holes in the active layers and, thus, limit the device quantum efficiency. To overcome the detrimental effects of these electrostatic fields the growth of nonpolar surfaces, such as *a*-plane $(11\bar{2}0)$ or *m*-plane $(1\bar{1}00)$, has been proposed.[9] In addition, the use of ZnO nonpolar surfaces has been stimulated by their inherently anisotropic structural and optical properties,[10] which have been exploited on surface acoustic wave devices[11] and ultraviolet light modulators.[12] Despite its technological importance no reports on nonpolar $Zn_{1-x}Cd_xO$ are found in the literature, while only Muthukumar *et al.*[13,14] have reported the growth of *a*-plane $Zn_{1-x}Mg_xO$ thin films. The growth was achieved on *r*-plane sapphire with an intermediate ZnO buffer layer (50 Å) that prevented the formation of rocksalt (Zn, Mg)O phases as well as polycrystalline $Zn_{1-x}Mg_xO$. Their x-ray diffraction study was mainly concerned with the anisotropic structural quality and only the perpendicular lattice parameter was evaluated, with no information concerning the in-plane strain state being provided.

In this paper we analyze the structural properties of *a*-plane $Zn_{1-x}Cd_xO$ alloys grown by metal-organic vapor phase epitaxy (MOVPE), the Cd concentration being determined by Rutherford backscattering spectrometry (RBS). The effect of increasing Cd concentration on the optical properties of the films has been evaluated by room-temperature photoluminescence (PL), while the evolution of the lattice parameters, perpendicular and in plane, with Cd incorporation has been established by high-resolution x-ray diffraction (HRXRD).

II. EXPERIMENTAL DETAILS

The $Zn_{1-x}Cd_xO$ thin films were grown in a two-inlet horizontal vent-run-type MOVPE reactor (Quantax 226 refurbished by EMF Ltd), operated at atmospheric pressure. Diethylzinc (DEZn), dimethylcadmium (DMCd), and tertiary butanol (tert-butanol) were used as Zn, Cd, and oxygen precursors, respectively, while N_2 was employed as carrier gas. The precursors were separately introduced into the reaction

[a]Electronic mail: jesus.zuniga@uv.es

chamber, the metal precursors through the upper inlet, and the alcohol through the lower one, reducing the gas-phase prereactions. Besides, the separate introduction of the precursors allows a better control over the precursors' partial pressures inside the reactor and results in a more homogeneous growth rate.[15]

The thin films were deposited on *r*-plane sapphire substrates (oriented to within ±0.5°), on which no chemical or thermal treatment had been performed. A ZnO buffer layer of around 800 nm was deposited prior to the alloy growth in order to prevent the appearance of rocksalt $Zn_{1-x}Cd_xO$ or CdO phases, similarly to Muthukumar *et al.*[13,14] The ZnO buffer was grown at 376 °C with a tert-butanol to DEZn molar ratio equal to 5. The growth temperature, as well as the tert-butanol and DEZn partial pressures, was maintained constant throughout the growth process, including the $Zn_{1-x}Cd_xO$ deposition. In order to achieve different Cd concentrations in the films, which were 1 μm thick, the DMCd partial pressure was progressively increased yielding DMCd/DEZn ratios from 0.075 to 0.43.

The composition of the $Zn_{1-x}Cd_xO$ films was determined by RBS using a 1.2 MeV proton beam with a diameter of 0.4 mm, and confirmed by particle-induced x-ray emission. The HRXRD measurements were performed in a Philips X'Pert MRD diffractometer employing a parallel incident beam coming from an x-ray mirror and a Bartels-type Ge(220) monochromator. The diffracted intensity was collected by a triple-crystal Ge(220) analyzer. PL emission was excited using the 325 nm line of a He–Cd laser with a spot diameter of around 100 μm.

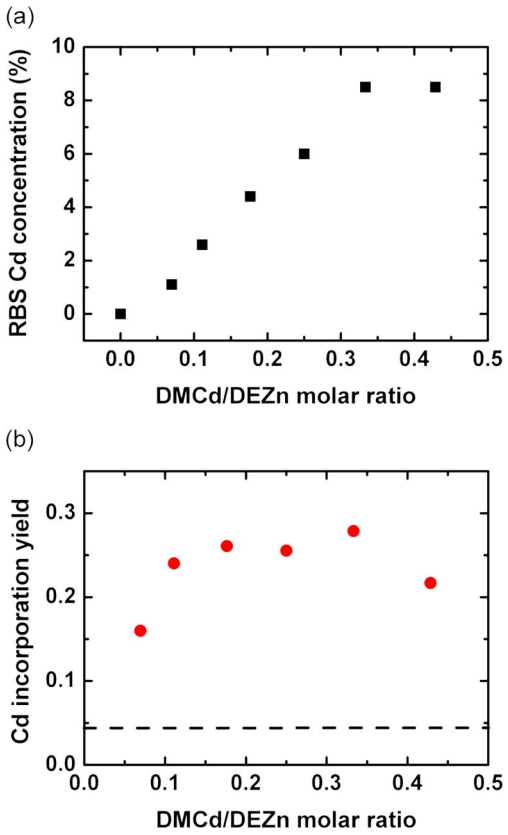

FIG. 1. (Color online) Cd concentration, in at. %, determined by RBS measurements (a) and Cd incorporation yield (b). The dashed line in (b) indicates the maximum Cd incorporation yield achieved in Ref. 7.

III. RESULTS AND DISCUSSION

A. Cd incorporation

The Cd concentration in the films shows a linear dependence on the DMCd partial pressure inside the reactor, as can be seen in Fig. 1(a). However, for DMCd to DEZn ratios around 0.35 the curve saturates, achieving a maximum Cd content in the order of 8.5 at. %. The Cd incorporation yield, which can be defined as the ratio between the Cd/Zn proportion in the film and the DMCd/DEZn proportion in the reactor, is depicted in Fig. 1(b). A yield value of 1 would mean that Cd and Zn incorporations are equally effective. For all compositions the incorporation yield is below unity, indicating a poorer Cd transfer from the gas phase into the film. Nonetheless, our yield results are at least three times higher than the maximum yield obtained on *c*-oriented samples grown with the same precursors.[7] The maximum yield in Ref. 7 is indicated by a dashed line in Fig. 1(b). Thus, the growth of *a*-oriented $Zn_{1-x}Cd_xO$ films seems to facilitate the Cd incorporation.

As we have mentioned in the Introduction, the incorporation of Cd into the ZnO lattice has been used to tune the emission wavelength of ZnO-based heterostructures into the visible. The band-gap decrease due to Cd incorporation can be monitored by PL measurements, although the near band-edge PL emission energy is lower than the actual band-gap energy due to Stokes' shift and the exciton binding energy.[8] Figure 2 shows a continuous decrease in the emission energy as more Cd is introduced, with a redshift of the PL peak of more than 300 meV for Cd concentrations around 8.5 at %. The emission energy dependence on Cd concentration deviates from a linear interpolation between the emission energies corresponding to the two pure binary compounds.[4,7,8] A second-order polynomial is required to reproduce the experimental results: $E_{\text{emission}}=(3.28-5.5x+16x^2)$ eV. The nonlinear fit reflects the band-gap bowing commonly observed in other II-VI alloys.[16,17]

For DMCd to DEZn ratios higher than 0.35 there is no additional Cd incorporation and the amount of Cd in the films, as determined by RBS, remains at 8.5 at. %. The RBS

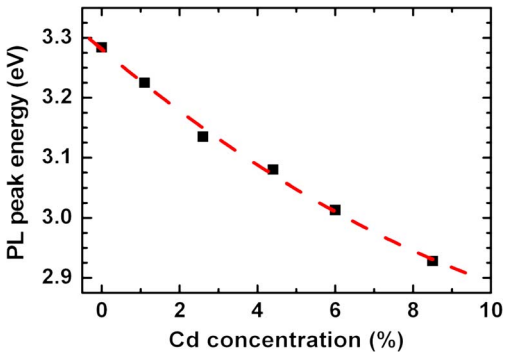

FIG. 2. (Color online) Cd concentration dependence of the room-temperature near band-edge PL emission energy of $Zn_{1-x}Cd_xO$ alloys. The dotted line, $E_{\text{emission}}=(3.28-5.5x+16x^2)$ eV, is the nonlinear fit of the experimental data.

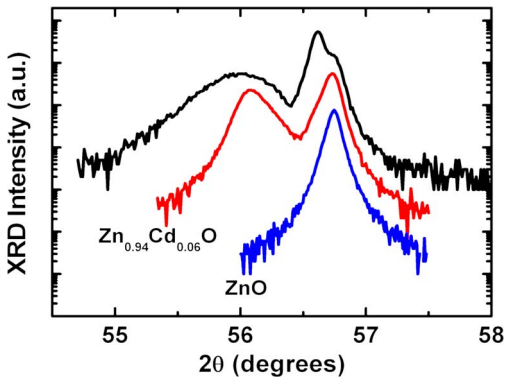

FIG. 3. (Color online) θ-2θ scans performed with a triple-crystal analyzer on pure ZnO, on a $Zn_{0.94}Cd_{0.06}O$ alloy and, on a $Zn_{1-x}Cd_xO$ layer grown with a DMCd to DEZn molar ratio of 0.43. The curves are shifted in intensity for clarity.

technique does not give directly the phase or phases composition, but informs about the relative abundance of each of the detected elements. Therefore, for DMCd to DEZn ratios higher than 0.35 the RBS measurements indicate that 8.5% of the cation sites are occupied by Cd atoms. The phases present within the sample must be determined using alternative techniques. In this sense, Fig. 3 shows the x-ray θ-2θ spectra of pure ZnO, of a $Zn_{0.94}Cd_{0.06}O$ alloy, and of a $Zn_{1-x}Cd_xO$ sample grown with a DMCd to DEZn ratio of 0.43. While the $Zn_{0.94}Cd_{0.06}O$ spectrum shows two peaks, the ZnO buffer peak at higher angles and the alloy peak at lower ones, the $Zn_{1-x}Cd_xO$ sample grown with a DMCd to DEZn ratio of 0.43 shows three peaks. The two peaks at lower angles correspond to two $Zn_{1-x}Cd_xO$ phases with different Cd concentrations, whereas the shoulder at higher angles comes from the ZnO buffer. Among the two phases, the $Zn_{1-x}Cd_xO$ alloy presenting a lattice parameter closer to the ZnO one shows a much narrower lattice parameter distribution. The 2θ full width of half maximum (FWHM) of this phase is 0.08°, instead of 0.45°, indicating a higher crystalline quality. The appearance of two $Zn_{1-x}Cd_xO$ phases, differing in the Cd concentration, was also detected in Ref. 7 and monitored by spatially resolved cathodoluminescence. Under the current growth conditions, 8.5 at. % seems to be the upper Cd concentration limit, above which phase separation takes place. In order to have Cd concentrations higher than 8.5 at. % other strategies should be used, such as growth conditions far from equilibrium.[8,18]

In the next section we will analyze the structural properties of the single phase $Zn_{1-x}Cd_xO$ films, that is, with Cd concentrations up to 8.5 at. %.

B. In-plane orientation and lattice description

The θ-2θ scans performed on receiving slit mode showed narrow peaks belonging to the sapphire $(01\bar{1}2)$ reflection, and one broad peak around $2\theta=56.6°$ which confirms that the films' growth direction is parallel to $[11\bar{2}0]$. If the measurement was repeated with a triple-crystal analyzer the broad peak was seen to split into two distinct peaks, one belonging to the $Zn_{1-x}Cd_xO$ alloy and the other to the ZnO buffer (see Fig. 3). Φ scans on asymmetric reflections,

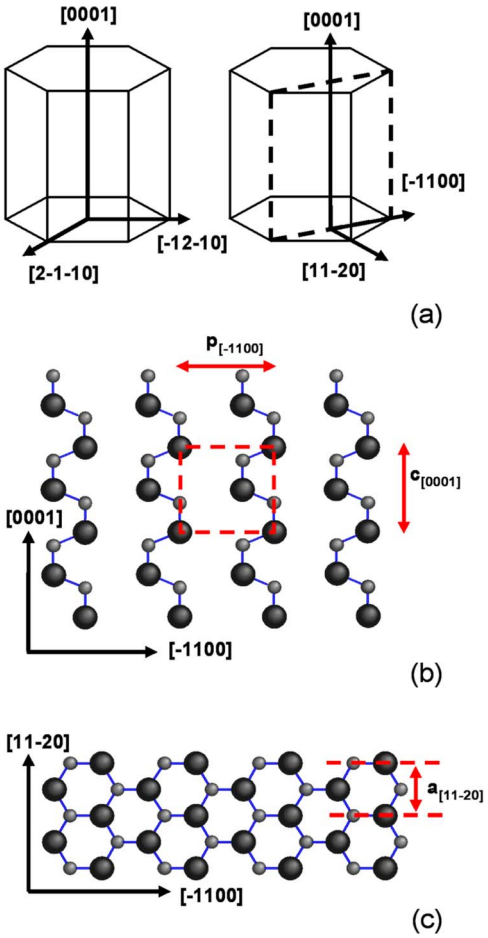

FIG. 4. (Color online) Reference frame commonly used in wurtzite materials (left) and new frame used for describing the lattice deformation of *a*-plane wurtzite materials (right) (a). Schematic top (b) and transversal (c) views of ZnO *a*-plane structure. The big and small spheres represent Zn and O ions, respectively. In the top view only one atomic plane has been represented, while in the transversal view along the [0001] axis two atomic planes have been considered (one containing only oxygen ions and the other containing only zinc ions).

namely, $ZnO/Zn_{1-x}Cd_xO\{10\bar{1}0\}$ and sapphire{0006}, were employed to determine the epitaxial relationships between the films and the *r*-plane sapphire substrates. Besides $Zn_{1-x}Cd_xO/ZnO(11\bar{2}0)\|$sapphire$(01\bar{1}2)$, we found $Zn_{1-x}Cd_xO/ZnO[0001]\|$sapphire$[01\bar{1}\bar{1}]$ and $Zn_{1-x}Cd_xO/ZnO[\bar{1}100]\|$sapphire$[2\bar{1}\bar{1}0]$. These results, which reproduce the in-plane orientation assumed by pure ZnO (Ref. 11) and $Zn_{1-x}Mg_xO$ (Ref. 13) on *r*-plane sapphire, are accurate except for a 180° rotation of the $ZnO/Zn_{1-x}Cd_xO$ lattice. The 180° uncertainty results from the insensitivity of the x-ray scans, performed with Cu $K\alpha_1$ radiation, to the polarity of the wurtzite ZnO structure. Alternative techniques, such as convergent beam electron diffraction, would be needed to determine accurately the epitaxial relationships in terms of polarity.[19]

To describe the lattice deformation induced on *a*-plane ZnO by Cd incorporation we shall refer all distortions to a new set of reference axes, as depicted in Fig. 4(a). The new axes are $[\bar{1}100]$, [0001], and $[11\bar{2}0]$. This axis transformation is equivalent to describing the lattice deformation in an

orthorhombic system rather than in the initial hexagonal one. The reference frame election is justified from a fundamental point of view by the surface atomic structure of *a*-plane ZnO, and from a practical point of view by the possibility of determining the periodicities along these axes independently. The surface structure of *a*-plane ZnO consists of ZnO dimers running parallel to [0001] and forming a zigzag pattern, as shown in Fig. 4(b). The distance between two of these zigzag curves is given by the periodicity along $[\bar{1}100]$ and will be referred to as "$p_{[\bar{1}100]}$", whereas the second in-plane periodicity gives directly the *c* lattice parameter, which is the distance between dimers along [0001]. The two in-plane reference axes are parallel to the sides of the surface unit cell, as indicated by a dashed line in Fig. 4(b). The periodicity along the third axis, which has been chosen to be parallel to the growth direction, will inform about the lattice deformation perpendicular to the surface. All three periodicities are indicated in Figs. 4(b) and 4(c), where schematic top and side views of the ZnO $(11\bar{2}0)$ surface are illustrated.

In order to independently determine these periodicities three different measurements have been performed. θ-2θ scans around the ZnO$(11\bar{2}0)$ reflection, employing the triple-crystal analyzer, provide the periodicity perpendicular to the surface, that is, $a_{[11\bar{2}0]}$. These scans were recorded twice, the difference being the in-plane direction, [0001] or $[\bar{1}100]$, contained within the scattering plane during the measurement. Meanwhile, to obtain the two in-plane periodicities reciprocal space maps (RSMs) around ZnO$(20\bar{2}0)$ and ZnO$(11\bar{2}2)$ reciprocal lattice points (RLPs) were recorded. From the first one, Fig. 5(a), we can deduce $p_{[\bar{1}100]}$ and $a[11\bar{2}0]$ since in this case the wave-vector components are measured along $[\bar{1}100]$ and $[11\bar{2}0]$. In the second RSM the wave-vector components are measured along [0001] and $[11\bar{2}0]$, so that $c_{[0001]}$ as well as $a_{[11\bar{2}0]}$ can be determined. Additionally, the perpendicular lattice parameter $a_{[11\bar{2}0]}$ can be used to assure the reliability of the measurements since the four obtained values, two from the θ-2θ scans and two more from the reciprocal space maps, should be equal after the proper tilt corrections.[20]

C. Lattice parameters

The experimental values of the in-plane and perpendicular periodicities, previously defined, have been plotted in Figs. 6(a)–6(c). For 0 at. % Cd concentration the value plotted for each of the three parameters is the average over all the ZnO buffer films plus the pure ZnO sample. These values reveal that the underlying ZnO is under tensile stress along $[\bar{1}100]$, with a strain of 0.40%, and under compressive stress along [0001], although in this direction the lattice is almost completely relaxed with a strain smaller than −0.03%. This anisotropic in-plane strain distribution has its origin in the epitaxial relationships adopted by the ZnO buffer on top of the *r*-plane sapphire substrates. The calculated lattice mismatch using the ZnO and sapphire bulk lattice parameters[21] along ZnO$[0001]\|$sapphire$[01\bar{1}\bar{1}]$ is 1.5%, while it increases up to 18.3% parallel to ZnO$[\bar{1}100]\|$sapphire$[2\bar{1}\bar{1}0]$. The lattice periodicities measured on the ZnO buffer films indicate that their thickness, 800 nm, is enough to release the strain along ZnO[0001] but that thicker buffer films are needed if complete relaxation shall be achieved parallel to ZnO$[\bar{1}100]$. Hence, the $Zn_{1-x}Cd_xO$ films are deposited on top of a uniaxially stressed ZnO template.

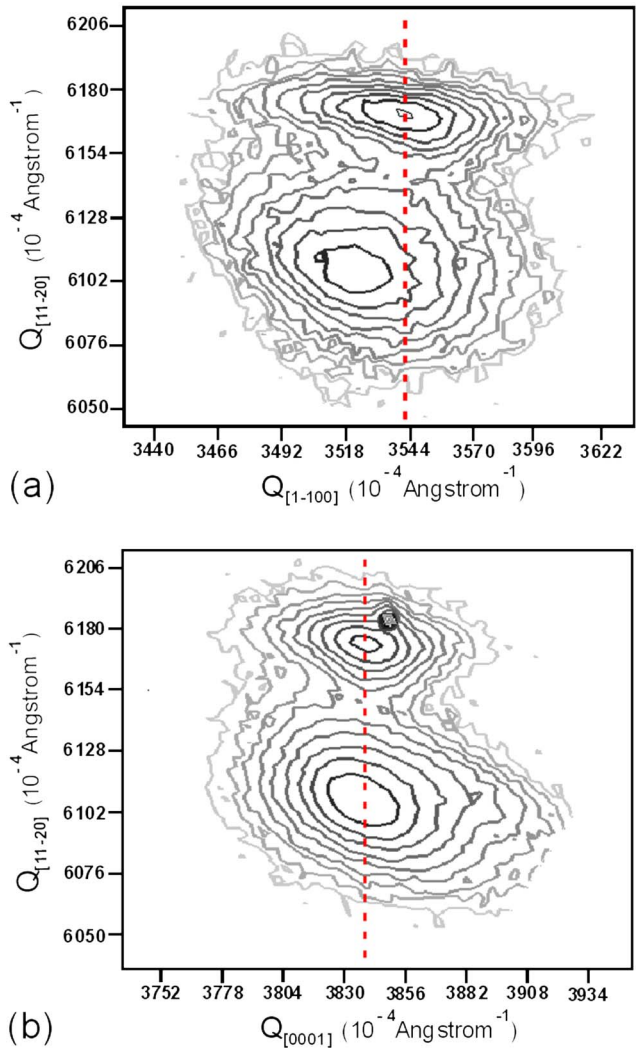

FIG. 5. (Color online) Reciprocal space maps taken on a $Zn_{1-x}Cd_xO$ sample, with $x=0.06$, around the ZnO (a) $(20\bar{2}0)$ and (b) $(11\bar{2}2)$ reflections. The vertical dotted line represents pseudomorphic growth.

Figures 6(a) and 6(b) show that for Cd content below 2.6 at. % the $Zn_{1-x}Cd_xO$ film grows pseudomorphically on the ZnO buffer, with both $Zn_{1-x}Cd_xO$ in-plane periodicities matching those of the stressed ZnO buffer. This pseudomorphic growth is maintained along the [0001] direction for all Cd concentrations, the $Zn_{1-x}Cd_xO$ $c_{[0001]}$ lattice parameter preserving the value imposed by the ZnO buffer. This can be seen for a $Zn_{0.94}Cd_{0.06}O$ alloy in Fig. 5(b), in which the $(11\ \bar{2}\ 2)$ RSM is shown. Irrespective of the Cd concentration the alloy RLP lies on the vertical line passing through the ZnO buffer RLP, indicating that the alloy periodicity along [0001] direction is the same as in the ZnO buffer. The biggest difference between the ZnO and the $Zn_{1-x}Cd_xO$ $c_{[0001]}$ lattice parameters for any Cd concentration is smaller than 0.1%, as seen in Fig. 7(a). The surface atomic structure is,

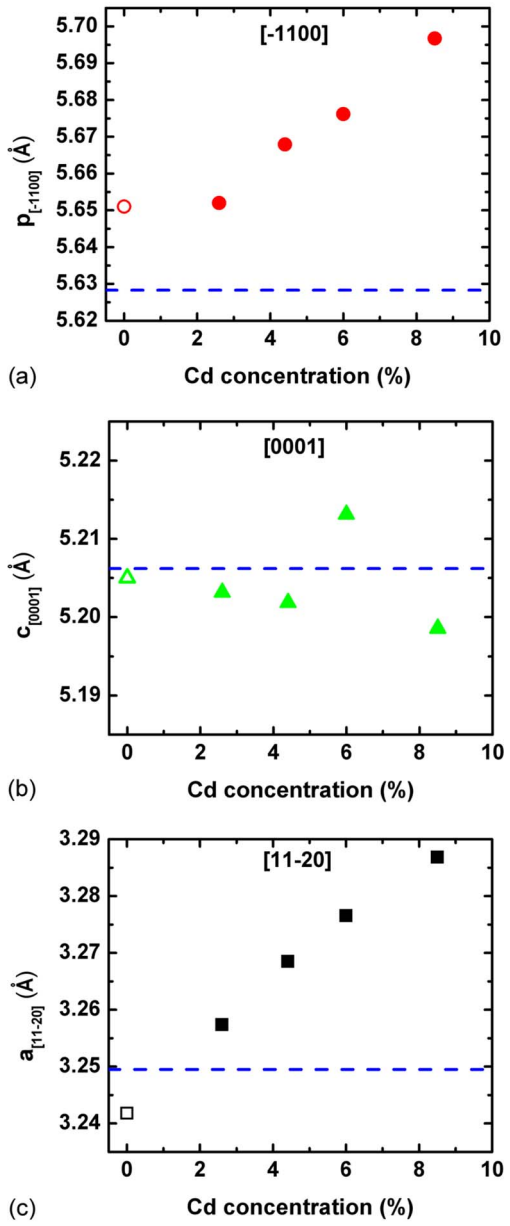

FIG. 6. (Color online) Lattice periodicities along (a) $[\bar{1}100]$ direction, (b) [0001] direction, and (c) $[11\bar{2}0]$ direction, as a function of Cd concentration. In all cases the dashed line represents the corresponding periodicity in bulk ZnO. The open symbols represent the ZnO lattice parameters averaged over all ZnO buffer layers plus the pure ZnO sample.

thus, not perturbed along the [0001] direction, with the mean dimer separation along [0001] being equal for any of the studied $Zn_{1-x}Cd_xO$ compositions. Hence, the stress due to Cd incorporation must be released along the two other possible directions.

Since for Cd concentrations below 2.6 at. % the $Zn_{1-x}Cd_xO$ surface unit cell mimics that of the underlying ZnO, the effect of Cd incorporation is an increase of the interplanar distance along the growth direction. This process breaks the sixfold symmetry of the alloy [0001] axis, see Fig. 4(c), and should be taken into account if optical devices are to be designed, since perturbations of the C_{6v} symmetry common to wurtzite materials are known to affect their optical properties.[22] For Cd concentrations higher than 2.6

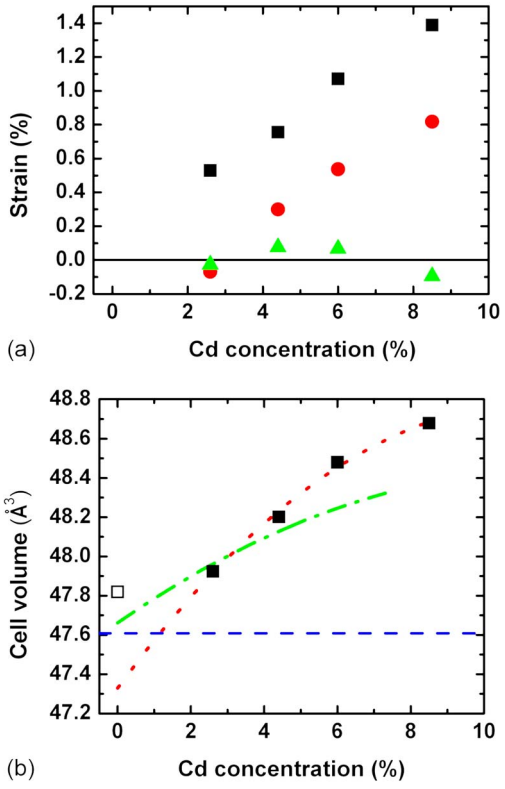

FIG. 7. (Color online) (a) Strain on $Zn_{1-x}Cd_xO$ as a function of Cd concentration along $[\bar{1}100]$ direction (●), [0001] direction (▲), and $[11\bar{2}0]$ direction (■). (b) Unit-cell volume as a function of Cd concentration. The open symbol represents the ZnO cell volume averaged over all ZnO buffer layers plus the pure ZnO sample. The dotted line is the quadratic fit to the experimental values, the dot-dashed line is the cell volume dependence found in Ref. 4, and the dashed line is the unit-cell volume of bulk ZnO.

at. % the stress perturbs not only the perpendicular lattice parameter but also the periodicity along $[\bar{1}100]$, as shown in Fig. 6(a). This expansion along $[\bar{1}100]$ implies that in the $(20\bar{2}0)$ RSM, shown in Fig. 5(a), the alloy RLP moves inside the relaxation triangle closer to the reciprocal space origin. For a Cd content of 2.6 at. % the alloy RLP lies on the vertical line, reproducing the pseudomorphic behavior detected along [0001]. However, as the Cd content increases the alloy RLP moves from the vertical line towards a diagonal line, at lower $Q_{[1\text{-}100]}$ values, associated to a completely strain-relaxed material in which the C_{6v} symmetry would be recovered. In terms of the atomic surface structure, the relaxation process increases the separation between the dimer zigzag rows and expands the surface unit cell along $[\bar{1}100]$.

In order to compare the effect of Cd incorporation along the three directions we define the strain in the $Zn_{1-x}Cd_xO$ film, along the $[ijhk]$ direction, as

$$\text{strain}_{[ijhk]}(Zn_{1-x}Cd_xO) = [p_{[ijhk]}(Zn_{1-x}Cd_xO) - p_{[ijhk]}(ZnO)]/p_{[ijhk]}(ZnO),$$

$p_{[ijhk]}(ZnO/Zn_{1-x}Cd_xO)$ being the periodicity along the $[ijhk]$ direction of the ZnO buffer and $Zn_{1-x}Cd_xO$ film, respectively. Figure 7(a) shows the strain in the $Zn_{1-x}Cd_xO$ as a function of Cd concentration. While the strain along [0001] is null, since the $Zn_{1-x}Cd_xO$ grows pseudomorphically along this direction, the strain parallel to $[11\bar{2}0]$ and $[\bar{1}100]$ shows

a linear dependence on Cd concentration. The slope of the fitting curves is found to be equal along both directions: 0.149(9), for strain parallel to $[11\bar{2}0]$, and 0.148(15), for strain parallel to $[\bar{1}100]$. The equality of the slopes indicates that the relative Cd-induced lattice deformation along $[11\bar{2}0]$ and $[\bar{1}100]$ is the same. The only difference between the two directions is the onset of lattice deformation, which is hindered along $[\bar{1}100]$ due to the presence of the ZnO buffer. For low Cd concentrations the ZnO buffer imposes its in-plane lattice parameters to the $Zn_{1-x}Cd_xO$ film, and therefore delays the surface unit-cell deformation along $[\bar{1}100]$. The overall effect is an increase of the unit-cell volume, Fig. 7(b), which shows a quadratic dependence with respect to Cd concentration $\mathrm{vol}([\mathrm{Cd}(\%)]) = (47.33 + 0.25^{*}[\mathrm{Cd}(\%)] - 0.011^{*}[\mathrm{Cd}(\%)]^2)$ Å^3. For comparison the unit-cell volume of *c*-oriented $Zn_{1-x}Cd_xO$ grown by pulsed laser deposition, Ref. 4, is also plotted as a function of Cd concentration. The maximum attained cell volume variation in the *c*-oriented samples before phase separation occurred was 1.5%,[4] while in our case it is 1.8%. The volume variation for 8.5 at. % Cd concentration extrapolated from the difference in Zn^{2+} and Cd^{2+} ionic radii, 0.14 Å, would be 2.25%. Thus, the presence of the stressed ZnO buffer, whose volume is in between that of pure ZnO and that of the $Zn_{1-x}Cd_xO$ alloys, reduces the Cd-induced lattice deformation and helps in increasing the range in which thermodynamically metastable[4] $Zn_{1-x}Cd_xO$ can be obtained.

IV. CONCLUSIONS

$Zn_{1-x}Cd_xO$ alloys have been grown on *a*-plane ZnO buffer films by MOVPE. The ZnO buffer films are uniaxially stressed along $[\bar{1}100]$, with complete relaxation being achieved along [0001]. These ZnO films serve as templates for the $Zn_{1-x}Cd_xO$ growth, in which a maximum Cd concentration of 8.5 at. % has been achieved. The 8.5 at. % Cd-containing alloy shows a near band-edge PL emission red-shifted more than 300 meV with respect to the pure *a*-plane ZnO.

For Cd concentrations below 2.6 at. % the $Zn_{1-x}Cd_xO$ grows pseudomorphically on the ZnO buffer, with stress being released by increasing the interplanar distance along $[11\bar{2}0]$. For higher Cd contents the lattice is deformed parallel to $[11\bar{2}0]$ and $[\bar{1}100]$, while the *c* lattice parameter remains unaltered. The $Zn_{1-x}Cd_xO$ lattice is progressively expanded until a volume variation of around 1.8% is attained at a Cd concentration of 8.5 at. %. Attempts for achieving higher Cd concentrations result in the appearance of two different $Zn_{1-x}Cd_xO$ compositions rather than phase separation into the pure binary compounds. Therefore, under near-equilibrium growth conditions, 8.5 at. % seems to be the Cd incorporation limit.

ACKNOWLEDGMENTS

This work was partially financed by the Spanish Government under Grant Nos. MAT2001-2920-C03, MAT2004-06841, and GV-Grupos 03/098, by the German Government under Grants German DFG within FOR 404, project A9, and SOXESS European Network. One of the authors (J.Z.) thanks the Spanish MECD for his predoctoral scholarship.

[1] A. Ohtomo *et al.*, Appl. Phys. Lett. **72**, 2466 (1998).
[2] A. Ohtomo, R. Shiroki, I. Ohkubo, H. Koinuma, and M. Kawasaki, Appl. Phys. Lett. **75**, 4088 (1999).
[3] T. Makino, C. H. Chia, N. T. Tuan, Y. Segawa, M. Kawasaki, A. Ohtomo, K. Tamura, and H. Koinuma, Appl. Phys. Lett. **77**, 1632 (2000).
[4] T. Makino, Y. Segawa, M. Kawasaki, A. Ohtomo, R. Shiroki, K. Tamura, T. Yasuda, and H. Koinuma, Appl. Phys. Lett. **78**, 1237 (2001).
[5] W. I. Park, G.-C. Yi, and H. M. Jang, Appl. Phys. Lett. **79**, 2022 (2001).
[6] R. Schmidt *et al.*, Appl. Phys. Lett. **82**, 2260 (2003).
[7] Th. Gruber *et al.*, Appl. Phys. Lett. **83**, 3290 (2003).
[8] A. Nakamura, J. Ishihara, S. Shigemori, K. Yamamoto, T. Aoki, H. Gotoh, and J. Temmyo, Jpn. J. Appl. Phys., Part 2 **43**, L1452 (2004).
[9] P. Waltereit, O. Brandt, A. Tranpert, H. T. Grahn, J. Menniger, M. Ramsteiner, M. Reiche, and K. H. Ploog, Nature (London) **406**, 865 (2000).
[10] C. Bundesmann, N. Ashkenov, M. Schubert, A. Rahm, H. v. Wenckstern. E. M. Kaidashev, M. Lorenz, and M. Grundmann, Thin Solid Films **455–456**, 161 (2004).
[11] C. R. Gorla, N. W. Emanetoglu, S. Liang, W. E. Mayo, Y. Lu, M. Wraback, and H. Shen, J. Appl. Phys. **85**, 2595 (1999).
[12] M. Wraback, H. Shen, S. Liang, C. R. Gorla, and Y. Lu, Appl. Phys. Lett. **74**, 507 (1999).
[13] S. Muthukumar, J. Zhong, Y. Chen, Y. Lu, and T. Siegrist, Appl. Phys. Lett. **82**, 742 (2003).
[14] S. Muthukumar, Y. Chen, J. Zhong, F. Cosandey, Y. Lu, and T. Siegrist, J. Cryst. Growth **261**, 316 (2004).
[15] R. Tena-Zaera, J. Zúñiga-Pérez, C. Martínez-Tomás, and V. Muñoz-Sanjosé, J. Cryst. Growth **264**, 237 (2004).
[16] J. E. Bernard, and A. Zunger, Phys. Rev. B **36**, 3199 (1987).
[17] A. Sotto, H. S. Güder, A Pérez-Pastor, A. Segura, J. Zúñiga, and V. Muñoz, High Press. Res. **22**, 257 (2002).
[18] S. Shigemori, A. Nakamura, J. Ishihara, T. Aoki, and J. Temmyo, Jpn. J. Appl. Phys., Part 2 **43**, L1088 (2004).
[19] M. D. Craven, S. H. Lim, F. Wu, J. S. Speck, and S. P. DenBaars, Appl. Phys. Lett. **81**, 469 (2002).
[20] J. M. Chauveau, Y. Androussi, A. Lefebvre, J. Di Persio, and Y. Cordier, J. Appl. Phys. **93**, 4219 (2003).
[21] F. Vigué, P. Vennéguès, C. Deparis, S. Vézian, M. Laügt, and J. P. Faurié, J. Appl. Phys. **90**, 5115 (2001).
[22] P. P. Paskov, T. Paskova, P. O. Holtz, and B. Monemar, Phys. Status Solidi A **190**, 75 (2002).